Received 20 June 2022 | Revised 12 July 2022 | Accepted 17 July 2022
Vol. 03, No. 01, 18 pages

RESEARCH ARTICLE

TUJES Tobruk University Journal of Engineering Sciences

Surface Treatment of Commercially Pure Titanium by Using Carbon Powder and Tungsten Inert Gas to Enhance Wear Resistance

Mustafa R. Alhawwari[1], Farag M. Shuaeib[1], Ezzeddin M. Anawa[2], and Thabet M. Elrabei[2]

[1] Mechanical Engineering Department, University of Benghazi, Libya
[2] Industrial Engineering Department, University of Benghazi, Libya
farag.shuaeib@uob.edu.ly

Abstract: The aim of the present study, is to perform a Tungsten Inert Gas (TIG) surface alloying of a Commercially Pure Titanium (C.P.Ti) substrate with carbon powder under an atmosphere of pure argon gas. Experiments were carried out to introduce larger amounts of carbon into titanium substrate using tungsten inert gas (TIG) as a heating source. The technique includes forming grooves of different depths on the surface of the titanium; these grooves were then filled with carbon powder and then remelt the surface with a high energy TIG arc at a statistically planned manner (Taguchi Design of Experiment–DOE). This process led to melting part of titanium and consequently, the carbon powder dissolved in the melted pool forming Ti-C alloyed zone. Optical microscope, XRD, and SEM were used to study the microstructure, morphology, and dimensions of the alloyed zones. Also, micro hardness measurements were conducted across the depth of the alloyed zone. Finally, reciprocating wear test were also conducted to study the wear performance of the surface alloyed specimens. In conclusion, it is found that modifying the surface of Commercially Pure Titanium (C.P.Ti) by this method produced a suitable surface layer which has high hardness. This high hardness improved the wear resistance of C.P.Ti and consequently could be used in applications where wear and erosion resistance are required.

Keywords: Welding, TIG, Wear.

1 Introduction

Titanium and its alloys are extensively used in aerospace, chemical, and marine industries, owing to their specific strength, good corrosion resistance, and high temperature properties [1]. However, poor tribological properties limit the usefulness of titanium alloy in many engineering applications [2]. Moreover, not all titanium and its alloys can meet all of the industrial and biomedical requirements. In order to improve the tribological, chemical, and mechanical properties, surface modification is often performed [3-4]. Up to date various surface modification techniques have been investigated for improving the wear resistance of titanium and its alloys [5-6]. These include carburizing, nitriding and oxidation [7-9]. Among them, carburization technique is one of the methods that can be used to form a hard ceramic coating on titanium alloys. The main objective of carburization is to provide a hard surface on titanium and its alloys for increasing wear resistance in articulation application since titanium carbide is one of the potential biocompatible carbide layers [10]. It is also one of the cost-effective surface modification methods to deliberately generate a carbide layer on

titanium alloy. Many researchers have reported that the carbide layer enables to increase hardness, wear resistance and corrosion resistance of titanium and its alloy [11]. Sintered solid titanium carbide is a very important non-oxide ceramics that widely used in the fields of wear resistance tools and materials due to its high melting point (3170 oC), low density, high hardness (2500 ~3000HV), superior chemical and thermal stability, and outstanding wear resistance. However, it is expensive and need special and advanced tools such as high temperature furnaces which might not be available commercially.

Apart from sintering, a titanium carbide layer can be created by other, which might be more cost effective, surface modification methods. This includes solid carburization (or high-temperature synthesis), gas-solid reaction (or gas carburization), sol-gel process plasma carburizing, carburization by laser melting/alloying, and finally carburization by TIG melting/alloying such as TIG melting with Si [12-15]. Among these methods, solid carburization process is considered as the simplest and the most cost-effective. However, in solid carburization, one of the main obstacles for TiC coating is the high affinity of titanium to oxygen, which leads to form TiO2 easily on the surface. To overcome this issue, vacuum carburization or inert gas environment should be introduced to remove O2 contents in carburization chamber [16]. Another common problem related to solid carburization is non-uniform hardness profile across the carburized layers due to the variation of carbon concentration in the surface region [17].

The above discussion of carburization showed four popular carburization methods, i.e. solid, gas, laser melting/alloying , and TIG melting/alloying. The last mentioned carburization method which uses the TIG as a heat source is the most promising cost effective method. This method was found to be very efficient and cost-effective for Cp-Ti surface modification using other alloying elements such as Si or carbon powders [18].

Also, most of the previous carburization methods research work were performed using the classical methods of changing one parameter (factor) at a time while holding the other parameters fixed. This methodology requires a lot of specimens and extensive experimental work, which is both costly and time consuming. Furthermore, this classical method is not capable of investigating the interaction effects between the factors and cannot be used to perform process optimization. All these drawbacks are tackled by using design of experiment (DOE) statistical methods such as the Taguchi and response surface methods. Reason for not using this method in the past is its complex mathematical formulation, which needs a lot of effort and time. These are facilitated by the current computer technological development and the generation of powerful statistical packages such as Minitab software [5-6].

In the process of TIG surface melting, a torch with adequate power density is passed over the surface of a substrate in which a large amount of energy is absorbed in a short time interval. This results in a liquid/substrate interface, which moves toward the substrate and within a fraction of a second, a molten pool region inside the substrate forms; due to the existence of temperature gradients across the surface layer and the underlying substrate. The TIG melt pool is rapidly solidified to form a layer with metallurgical bond to the substrate material. Short processing time; flexibility in operation; economy in time, energy, and material consumption; and processing precision are the important advantages of TIG surface alloying process. Limited works are reported on the applications of this process for surface modification of titanium alloys [19-20]. Therefore, the aim of the present study, is to perform a TIG surface alloying of a preplaced C.P.Ti substrate with carbon powder under an atmosphere of pure argon gas. The Taguchi method would be used to plan the experiments. Then the produced specimens would be subjected to an extensive metallurgical and tribological investigation.

2 Materials and Methods

In this work, the effect of some important parameters such as current, speed, groove and arc length were investigated by using design of experiment approach. Taguchi Method in the design of experiment (DOE) was utilized to perform the parametric studies, and to determine the optimum TIG alloying setting. Based on literature review, four variables were chosen in preparing for the experiment and 3 levels were selected and inserted into the program as shown in the Table (1). The selected parameters are the welding current, the speed of welding, the depth of the cavity filled with carbon powder and arc length of the weld.

Table 1. Welding factor values at different levels.

Name	Unite	Levels	L (1)	L (2)	L (3)
Current	Ampere	3	100	130	160
Speed	mm/ min	3	100	150	200
Groove	mm	3	1	1.75	2.5
Arc length	mm	3	2	2.5	3

This was done after careful study and reference to previous studies and knowledge of the most variables that affected the characteristics of the metal and give the required results. After completing these requirements the design matrix generated as shown in Table (2).

Table 2. The design matrix.

Run	Factor 1 A: Current Ampere	Factor 2 B: Speed mm/min	Factor 3 C: Groove mm	Factor 4 D: Arclength mm
1	160	200	1.75	2
2	100	150	1.75	2.5
3	130	200	1	2.5
4	160	100	2.5	2.5
5	100	100	1	2
6	100	200	2.5	3
7	130	100	1.75	3
8	130	150	2.5	2
9	160	150	1	3

Specimens with a diameter of 20 mm and a thickness of 10 mm of commercially pure titanium (C.P.Ti) were used. Specimens were grooved in the middle of the specimen surface with different depths as shown in Fig. ((1) -a) and the carbon powder was added in the grooves. After preparing the specimens and filling the grooves with the carbon powder, specimens were then fixed on the workbench and the argon protection system was prepared to prevent oxidation during the welding process that may cause cracks of the specimen surfaces. Pure argon with the flowing rate of 15 l/min was purged into the operation chamber. Surface alloying is carried out using a TIG torch traversing the CP-Ti substrate and a series of single track without overlap were produced. The speedometer was used in the alloying process because it is found that welding speed is an important parameter for effective results (See Fig. (2)). The TIG welding/alloying machine features were argon gas flow rate of 6 l/min, non-consumable W electrode with 2.4 mm diameter, DC supply of about 100─160 A, voltage of 15 V, and substrate traverse speeds of 100-200 mm/min. The arc length was 2-3 mm. The Groove depth was 1-2.5mm and the electrode polarity was chosen as DCEN (Direct current electrode negative).

Various alloyed tracks were produced according to the design points shown in Table (2). The specimens were then ground down using emery paper grades from 120 up to 1,200. The specimens were polished using alumina powder ranging from (0.6, 0.3 and 0.1 µm) in sequences as shown in Fig. ((1)-b). Some of the specimens shows some distortion due to the heat of TIG process. Specimen number is not appearing here as it is in the side of the specimen. The microstructure of the TIG surface alloyed tracks was studied using optical and scanning electron microscopes (SEM). The crystal structure of the TIG surface alloyed specimens was investigated by X-ray diffraction (XRD) using Cu radiation generated at 40 kV and 30 mA.

A microhardness tester equipped with a Vickers diamond pyramid indenter was used for microhardness measurements along the depth of the transverse sections of the TIG alloyed specimens. The hardness was measured by employing mitutoyo microhardness tester MVK-HVL with a Vickers diamond available in Libyan Petroleum Institute in Tripoli. A 500g load was applied on the indenter. The wear loss of the TIG surface alloyed specimens and untreated substrate was measured using a sliding wear testing apparatus. The wear tests were performed at ambient temperature under dry conditions, normal load of 25 N, sliding speed of 0.5 ms–1, and a sliding distance of 0.1 m (see Fig. (3)).

(a) (b)

Fig. 1. Titanium specimens (a) before with grooves cut and (b) after surface treatment.

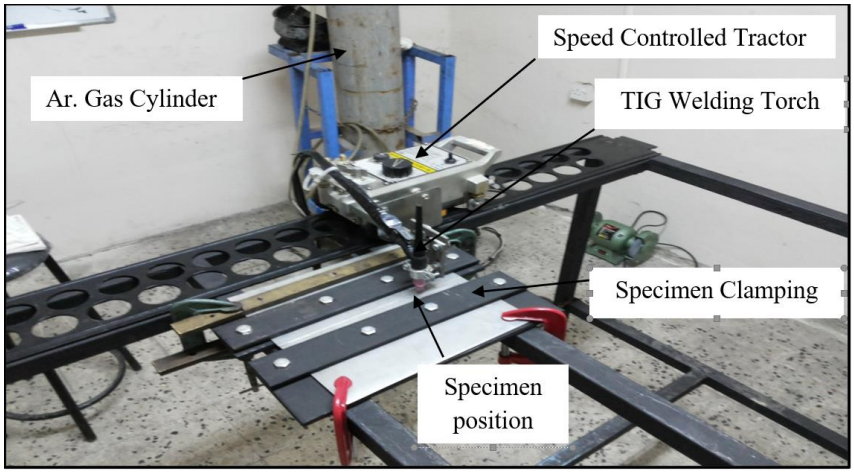

Fig. 2. Experimental set-up for TIG surface alloying.

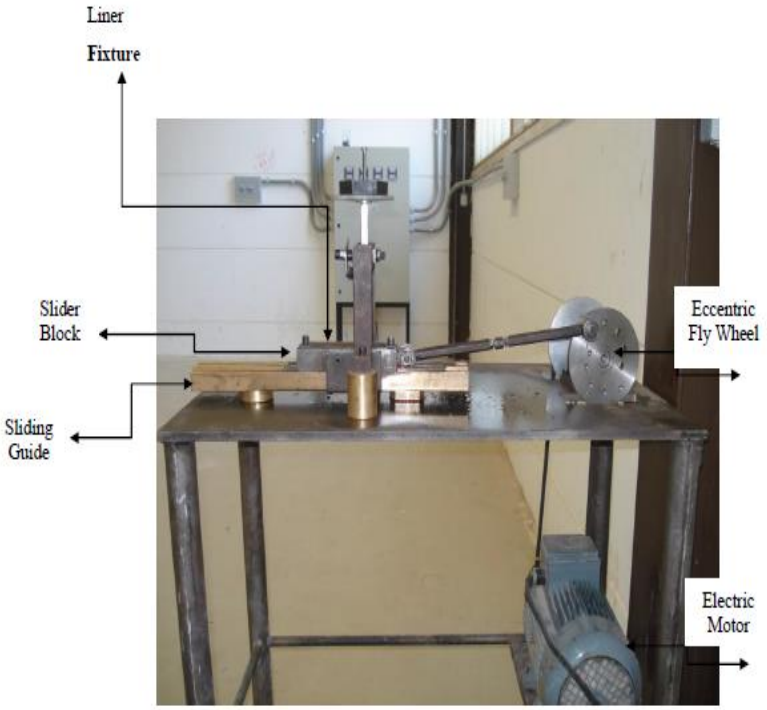

Fig. 3. Sliding wear test apparatus.

3 Results

In the beginning, heat input analysis, microscopic structure of the metal using an ordinary optical microscope and scanning electron microscopy (SEM) and X-ray diffraction (XRD) investigation were caried out. After that, the results of the DOE design program in terms of hardness and wear, which is a modern and useful method in the science of statistics is presented and discussed. The DOE method gives us the best conditions to obtain the best hardness and less wear at lower costs and reduce the error rate in experiments due to random selection of factors.

3.1 Heat Input Analysis

This study is based on the following factors: current intensity (A), welding travel speed (S), voltages (V) and arc length. It is well known that the welding process introduces large amounts of heat to dissolve the surface to ensure the spread of carbon particles. From equation (1) we can calculate the amount of heat entering. Table (3) shows the values of thermal inputs used in our experiments [19].

$$\text{Heat input (J/ mm)} = [\eta^* (A) * (V)] / (S) \qquad (1)$$

Where:
η: thermal efficiency constant of argon gas =0.65
A: Current Intensity (Amp).
V: Voltages (V).
S: Welding Travel Speed (mm/s).

The different values for the introduction of heat related to design points (1 to 9). By increasing the thermal input, the substrate gradually melts (giving more dilution) increases the Ti and decreasing the carbon content. Because of the energy that is absorbed mainly which is acting on evaporation of carbon powder.
We also note that when increasing the thermal input with increasing the depth of the groove we get a high hardness as in specimen No. 4 because the amount of thermal input gave a large carbon permeability to fit with the depth of the groove and thus be the TiC phase as shown in the scanning electron microscope.

Table 3. The values of thermal inputs used in the experiments.

Track No.	Current Intensity (Amp)	Voltage (V)	Welding Travel Speed (mm/s)	Groove mm	Heat input (J/mm)
1	160	15	3.33	1.75	468
2	100	15	2.50	1.75	390
3	130	15	3.33	1	380.25
4	160	15	1.67	2.5	936
5	100	15	1.67	1	585
6	100	15	3.33	2.5	292.5
7	130	15	1.67	1.75	760.5
8	130	15	2.50	2.5	507
9	160	15	2.50	1	624

3.2 Microstructure Analysis

Optical microscope. As an essential part of this study, the microstructure of the treated specimens were investigated using an optical microscope (X1000). First, test was performed for a non-treated specimen (carbon free) as shown in Fig. (4). Then all the specimens were tested for the presence of carbon as compared to the untreated specimen as shown in Figs (5 & 6) for specimens No. 2 and 4 respectively.

Fig. 4. Microstructure of commercially pure titanium (C.P.Ti) without adding carbon (X1000).

Fig. 5. Microstructure of Specimen No. 2.

Fig. 6. Microstructure of Specimen No. 4.

Scanning Electron Microscopy (SEM). The electron microscopy (SEM) test for all specimens was conducted. SEM, despite its higher cost, is more accurate than optical microscope because the output of the optical microscope could not explain the form of the titanium carbide Phase (TiC) accurately. At first, it was observed that throughout the specimens there is no porosity and more important there is no cracks that may grow and cause the catastrophic collapse of the material. Cracking was one of the major problems of CPTi surface alloying in the past. The original CPTi metal (without adding carbon) was also SEM examined to compare it with the carbon added specimens as shown in Fig. (7). From the microstructural results of the scanning electron microscopy (SEM), it was found that the titanium carbide phase in the form of dendritic and spherical phases were present in all specimens that were treated with the addition of carbon as shown in the Figs. (8 & 9).

The cellular-dendritic structure (showing secondary arms) observed is a result of the breaking-up of the planar solidification front due to the occurrence of constitutional super cooling in the liquid ahead of the interface which depends on the ratio of G/R (Temperature Gradient/ Solidification Rate). At the onset of solidification, G has its highest value and R = 0, the planar front forms at the highest values of G/R. As solidification proceeds, the G decreases and R increases, so that G/R decreases and cellular dendritic structure forms. The higher the heat input the coarser the dendrites. In Fig. (10), a typical microscopic (SEM) analysis of a titanium specimen illustrates the titanium carbide phase in the spherical and dendritic form. This figure was added here for comparison purposes noting the larger magnification factor of it.

The microscopic images of the scanning electron microscopy (SEM) are shown in specimens treated with carbon as shown in the selected Figs. (8 & 9). It is observed that the microstructure of the treated area consisted mainly of the (TiC), spherical and dendritic particles of the martensite matrix. Therefore, this process led to melting the carbon in the grooves with the specimen in it, which led to the diffusion of carbon in the specimen. Due to the low melting of carbon in beta titanium β-Ti, titanium carbide (TiC) particles were formed during deposition. In the initial phase of hardening where the carbon content of the surface was high, titanium carbide (TiC) was formed and then the amount of melting of the carbon began to decrease to the point of the eutectic, the point at which the mixture solidifies at one temperature.

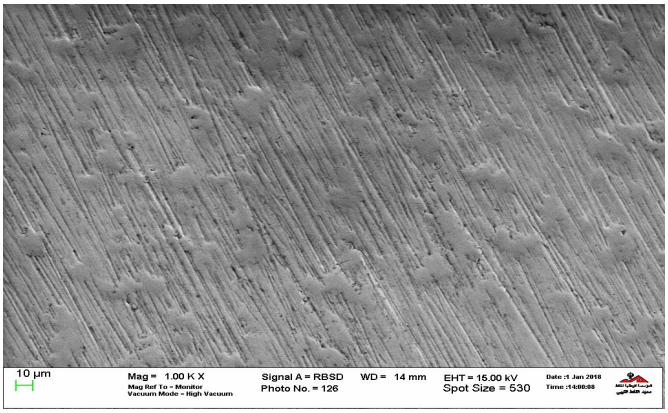

Fig.7. SEM, scanning electron micrograph of surface alloy for commercially pure titanium without any surface treatment (alloying).

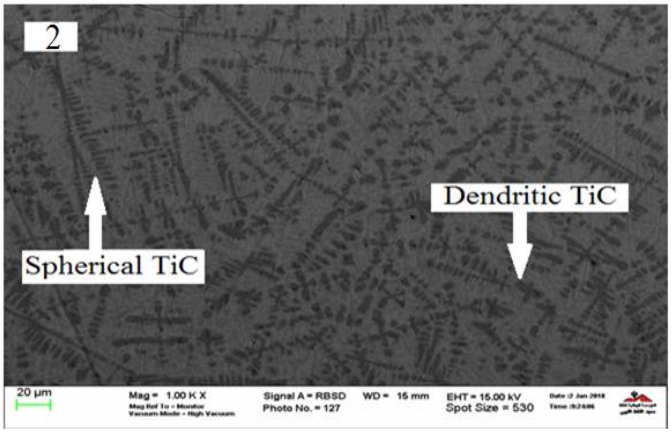

Fig. 8. SEM, scanning electron micrograph of surface alloy for specimen No. (2).

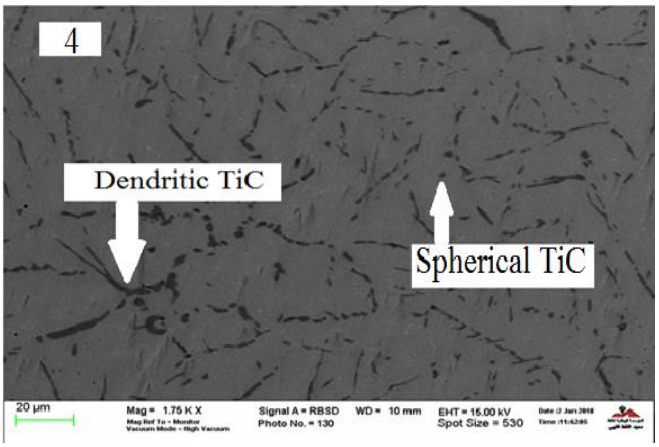

Fig. 9. SEM, scanning electron Micrograph of surface alloy specimen No. (4).

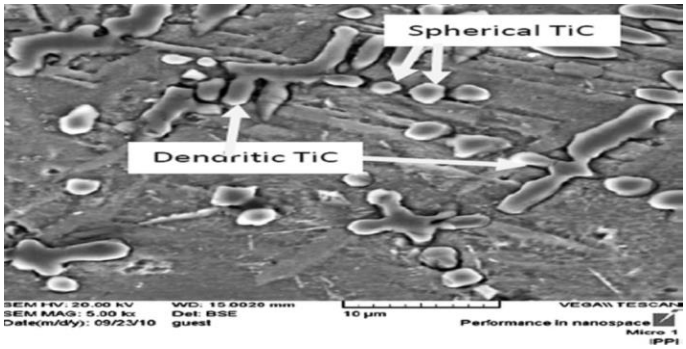

Fig. 10. SEM photo of the typical structure of titanium carbide from one of the scientific references to compare with the results (Larger magnification) [19].

X-ray Diffraction Analysis. From the previous section, during the study of the microscopic structures of the specimens, we clearly showed the shape of the titanium carbide (TiC) phase. And to find out the percentage amount of this phase in each specimen the X-ray diffraction test was conducted for all the specimens. The most hardened specimens were those containing high percentages of titanium carbide (TiC). The specimen No. (2) was the hardest, and the ratio of titanium carbide (TiC) was 19% as shown in Fig. (11), and then followed by The specimen No. (4) where the ratio of titanium carbide (TiC) was 13.22% as shown in Fig. (12).

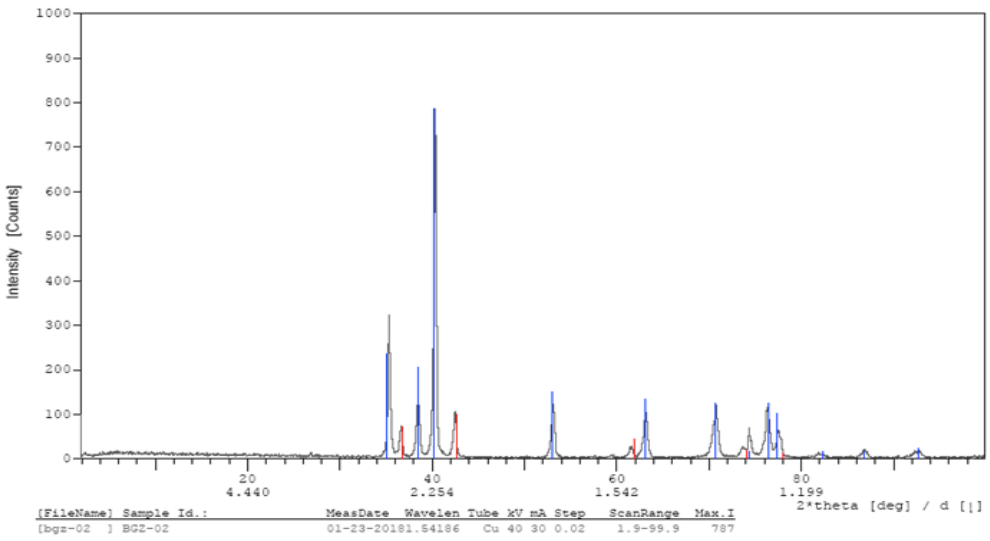

1	**Ref. Code**	**Compound Name**	**Chemical Formula**	**Quant [%]**
	05-0682	Titanium	Ti	81
	38-1420	Titanium Carbide	TiC	19

Fig. 11. X-ray diffraction and semi quantitative analysis table of specimen No. (02).

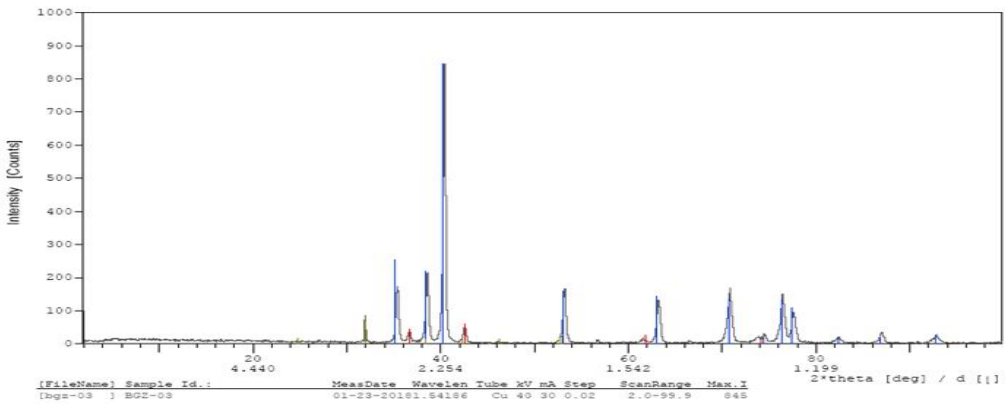

1	Ref. Code	Compound Name	Chemical Formula	Quant [%]
	05-0682	Titanium	Ti	86.78
	38-1420	Titanium Carbide	TiC	13.22

Fig. 12. X-ray diffraction and semi quantitative analysis table of specimen No. (4).

3.3 Microhardness Analysis

Using design of experiments (Taguchi method), results were obtained as shown in Table (4), and then analyzed as shown in Table (5). The effect of each variable in the surface treatment process and here its effect on the hardness of the metal were generated. The original (untreated metal) was measured to be 160HV0.5 and the maximum hardness value obtained in this work was 738HV0.5 . This result means that we obtained a high hardness ranging from 4 to 5 times from the untreated original specimen.

Table 4. The actual design of the matrix complete with hardness response inserted.

Run	Factor 1 A: Current Amp	Factor 2 B: Speed mm/min	Factor 3 C: Groove mm	Factor 4 D: Arclength mm	Response 1 Micro hardness HV
1	160	200	1.75	2	460
2	100	150	1.75	2.5	738
3	130	200	1	2.5	501
4	160	100	2.5	2.5	713
5	100	100	1	2	486
6	100	200	2.5	3	520
7	130	100	1.75	3	403
8	130	150	2.5	2	561
9	160	150	1	3	451

The determining factor (R^2) indicates the goodness of fit of the model. The value of R^2 of this model is 99.95 %, which is greater than 80%. This implies that at least 99.95 % of the variability in the data for the response is explained by the model. This indicates that the proposed model is adequate. Analysis of the response regression model was carried out using analysis of variance (ANOVA. The analysis results for the model,

are shown in Table (5). If "P" value is less than 0.05, the corresponding factor have significant influence on the response, at 95% confidence level.

Table 5. Analysis of variance.

Source	Sum of Squares	df	Mean Square	p-value Prob> F	
Model	1.0735E+005	7	15335.71	0.0439	Significant
A-Current	47040.00	1	47040.00	0.0207	
B-Speed	12060.17	1	12060.17	0.0409	
C-Groove	21122.67	1	21122.67	0.0309	
D-Arc Length	12604.17	1	12604.17	0.0400	
AC	9660.50	1	9660.50	0.0457	
BC	57600.00	1	57600.00	0.0188	
$A^{\wedge 2}$	49665.33	1	49665.33	0.0202	
Residual	50.00	1	50.00	0.0439	
Cor Total	1.074E+005	8	15338.57	0.0207	
R-Sq = 0.9995			R-Sq (adj) = 0.9963		

Microhardness 3D Surface Plot and Contour Analysis. After model building and verification, the Taguchi model is used to generate plots which relate the microhardness (response in this study) with the independent variables (factors) which are the current (Ampere), speed (mm/min), groove (mm), and arc length (mm). Part of these plots are generated and discussed hereafter. However, it is to be remembered that reading the 3D surface and contour graphs need some sort of careful attention as not to withdraw any misleading or conflicting conclusions. To simplify interpreting the results, the effect of each two factor will be considered as they are exists separately and then the overall interpretation of the whole plots will be made.

Fig.(13) shows the 3D surface plot and the contour plot of the effects of the current A in Amperes and the groove C in mm on the microhardness (Response) of the TIG Carburized (C.P.Ti) surface. As shown by the 3D surface plot, by increasing the current beyond 100 Amperes the surface hardness decreased. This hardness decrease continues until the current reached reaches about 150 Amperes, where increasing the current further, the hardness start increasing. Therefore, according to this plot a (maximum) microhardness setting is achieved with the current value around 100Ampers. Regarding the effect of the TIG surface alloying groove size as shown in Fig.(13) increasing the groove size from the lower level of 1 mm to the higher level of 2.5 mm the hardness has shown an almost with a maximum hardness close to the 2.5mm groove size. This is evident from the upward curved surface of the groove side of the 3D surface plot.

This is supported by the contour plot of Fig. (14) where it is also evident from the colored regions of the (1200 HV0.5) value which can be achieved by varying both the current and groove. It is to be noticed that the (1200 HV0.5) contour lines are achieved with both lower and higher current ranges, while for moderate current lower hardness is achieved. This agrees very well with 3D surface plot finding just mentioned above. However, the contour plot also shows that very high groove would result to higher hardness which is clear from the (1200 HV0.5) contour lines.

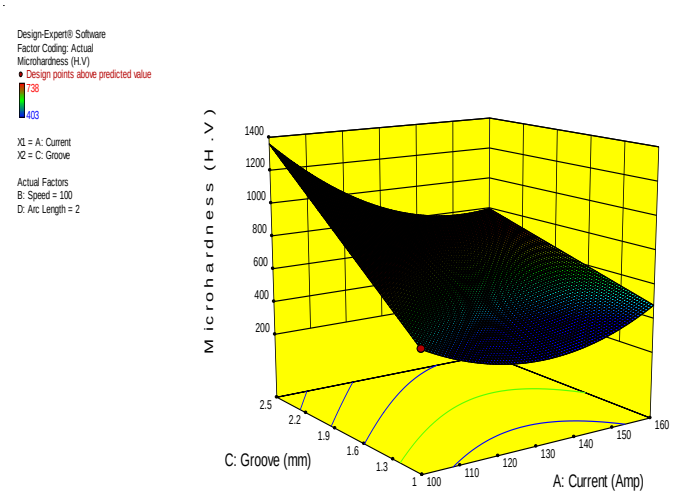

Fig. 13. 3D surface plot showing the combined effects of A and C on Microhardness when B is kept constant at (100mm/min) and Arc length= 2 mm.

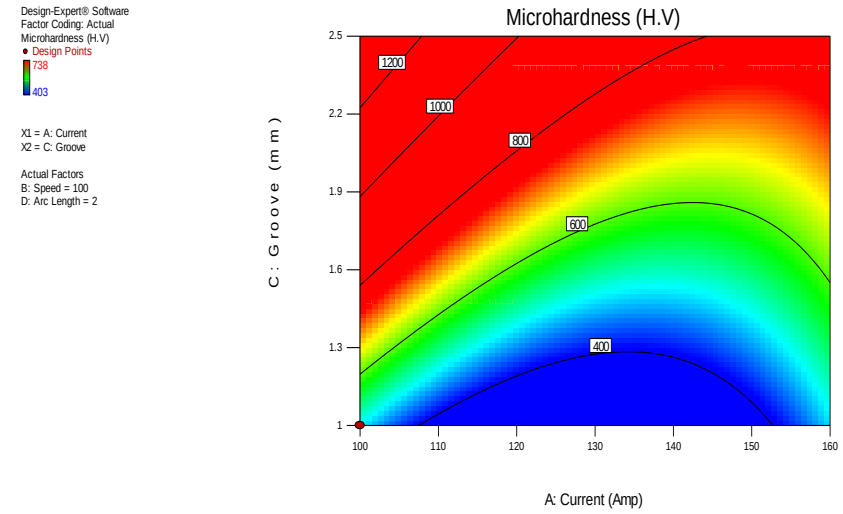

Fig. 14. Contour plot showing the combined effects of A and C on Microhardness when B is kept constant at (100mm/min) and Arc length= 2 mm.

3.4 Optimization of The TIG Process Parameters Individual Response (Microhardness)

The previous section has provided a comprehensive analysis on the effect of the selected process parameters on the surface hardness of the TIG Carbide titanium material. From the previous section, the optimum setting of the TIG power was mostly evident. However, the optimum settings of current, groove, speed and the arc length could not be very well defined from these plots and therefore the maximum hardness setting as determined by the optimization chart is required. This chart is produced by the response optimizer of the Design Expert program (Taguchi method). The achieved results were based on the different criteria's presented in Table (6). The chart predicts that the optimum process parameters settings are current= 95

Ampers, speed= 100.076 mm/min, groove = 2.473 mm and arc length= 2 mm as shown in the Table (7) which would result in a maximum predictable microhardness of 1460.054 HV0.5.

Table 6. The optimization criteria for input/output welding parameters (HV).

Parameter		W. Current	W. Speed	Groove	W. Arc length	Microhardness H.V
1	Criteria	Max.	Min.	Max.	Min.	Max.
	Importance	+ + +	+ + +	+ + +	+ + +	+ + + + +
2	Criteria	Min	Min	Max.	Min.	Max.
	Importance	+ + +	+ + +	+ + +	+ + +	+ + + + +
3	Criteria	In Range	In Rang	In Range	In Range	Max.
	Importance					+ + + + +

Table 7. The numerical optimization results based on individual response (HV).

	Parameter	Current	Speed	Groove	Arc length	Response Value	Desirability
1	Microhardness	179.734	100	2.5	2	956.894	0.999
2	Microhardness	95	100.076	2.473	2	1460.054	0.997
3	Microhardness	98.199	108.117	2.368	2.786	1132.286	1

3.5 Wear Resistance

It is assumed that the wear process proceeds by preferentially abrading the matrix and pick and dig up the matrix progressively. This action gradually raises the hard TiC particles in the coating and then these particles carry the load of abrasive particles [20]. Generally, the two components of wear resistant materials (matrix and hard particles) perform different roles. While the metal matrix supplies sufficient toughness for hard particles, the hard particles provide a barrier against indentation, grooving and cutting of abrasive materials as well as reducing the contact area of the matrix with the abrading counter face. Thus, the amount, size and distribution of hard particles and also the hardness and fracture toughness of both components and the bond between them are significant parameters in the resistance of material against wear [21]. Wear mechanism typically classifies into four types of interactions between abrasive particle and a wearing material, namely micro ploughing, micro fatigue, micro cutting and micro cracking. Micro ploughing does not lead to any material separation from the wearing surface because of a single pass of one abrasive particle. A plow is produced ahead of the abrading particle and the material is successively moved sideways to create ridges adjacent to the groove. The material may break off by micro fatigue as a result of plowing aside repeatedly by passing particles. Micro cutting produces a volume loss by chips equal to the volume of wear grooves. Micro cracking takes place when abrasive particles impose on highly concentrated stresses, especially on the surface of brittle materials. Generally, micro ploughing and micro cutting are the major mechanisms that occur in ductile materials while micro cracking is dominant on brittle materials [22].

Using equation (2), we can measure the specific wear rate after each time period. At the end the arithmetic average of the wear rate is taken. All carbon-treated and non-carbonated specimens were tested for comparison only, and results are shown in the Table (8). Then the final outputs of wear (Response 2) on the program design of experiments (Taguchi method) are inserted shown in the Table (9). To get the best operating conditions that we can use and the lowest possible costs and compare with the previous response (Response 1 : Microhardness) [23].

Given: FN = 25 N; v = ω×r; ω= 5rev/s ; r = 0.1m

∴ v = 0.5m/s ;

ρ = 4.55 × e-6 Kg/mm3

$$Ws = \Delta m / (FN.v.\rho.\Delta t) \quad (2)$$

Where: Ws = specific wear rate(mm3/N.m), FN = applied normal force (N), v = velocity(m/s), ρ=density, (kg/mm3), Δm = mass loss (kg), and Δt = time interval (s).

Similarly, the determining factor (R^2) indicates the goodness of fit of the model. The value of R^2 of this model is 98.36%, which is greater than 80%. This implies that at least (98.36%) of the variability in the data for the response is explained by the model. This indicates that the proposed model is adequate.

Analysis of the effects on the welding parameters in more details was carried out using analysis of variance (ANOVA) with implementing the regression method using Design Expert software. The analysis results for the reduced linear model, which is suggested by the software for the calculated specific wear rate values are shown in Table (10). If "P" value is less than 0.05, the corresponding factor is to have significant influence on the response, at 95% confidence level.

Table 8. Specimen weights before and after the test.

NO	Before	After					
		Weight (mg)					
	Weight (mg)	5 (min)	10 (min)	15 (min)	20 (min)	25 (min)	30 (min)
1	14545.4	14542.5	14541.5	14541.0	14526.3	14525.1	14523.1
2	14698.5	14692.9	14687.7	14685.5	14678.3	14673.3	14670.3
3	12965.4	12963.8	12962.7	12961.1	12960.0	12958.0	12956.9
4	14298.4	14291.9	14273.0	14270.0	14266.5	14265.4	14263.4
5	13461.4	13458.6	13457.2	13455.7	13454.3	13453.0	13451.0
6	14028.4	14025.4	14018.0	14015.5	14012.7	14011.2	14010.7
7	17009.1	17003.1	16997.0	16989.4	16983.9	16978.4	16975.1
8	15565.3	15560.2	15555.0	15549.1	15544.3	15539.2	15534.5
9	13526.2	13522.0	13520.00	13513.1	13509.5	13508.0	13506.3
Standard Specimen	15555.6	13526.8	12326.5	11645.3	10754.8	9876.8	91254.3

Table 9. The actual design of the matrix complete with specific wear rate inserted.

Run	Factor 1 A: Current Amp	Factor 2 B: Speed mm/min	Factor 3 C: Groove mm	Factor 4 D: Arclength mm	Response 2 Specific wear rate ($mm^3/N \cdot m$)
1	160	200	1.75	2	184.32
2	100	150	1.75	2.5	29.431
3	130	200	1	2.5	84.32
4	160	100	2.5	2.5	47.954
5	100	100	1	2	117.13
6	100	200	2.5	3	222.92
7	130	100	1.75	3	358.8
8	130	150	2.5	2	305.36
9	160	150	1	3	222.76

Table 10. Analysis of variance.

Source	Sum of Squares	df	Mean Square	p-value Prob > F	
Model	1.026E+005	6	17104.74	0.0485	Significant
A-Current	37739.18	1	37739.18	0.0220	
B-Speed	174.14	1	174.14	0.6963	
C-Groove	3851.88	1	3851.88	0.1681	
D-Arc Length	6512.24	1	6512.24	0.1103	
BC	65749.05	1	65749.05	0.0128	
A^2	65759.67	1	65759.67	0.0128	
Residual	1714.31	2	857.16		
Cor Total	1.043E+005	8	17104.74		
R-Sq = 0.9836			R-Sq (adj) = 0.9343		

3.6 Multiple-Response Optimization Using Taguchi Method

In practical industrial applications a total optimization may be desired, for this reason a multiple-response could be a solution. Multiple-response (all input/output welding parameters) optimization can be achieved using the optimization process in the Design-Expert software in the search for a combination of factor levels that simultaneously satisfy the requirements placed (i.e. Optimization criteria) on each one of the inputs/output welding parameters.

The goals are combined into an overall desirability function and the optimization performed can be numerical and/or graphical optimized. Numerical and graphical optimization methods were used in this research by selecting the desired goals for each factor and response. The numerical optimization process involves combining the goals into an overall desirability function (D). The numerical multiple-response optimization criterion is to reach maximum Hardness, Minimum Wear rate, with minimizing welding current, minimizing welding speed, maximizing Groove and minimizing Arc length.

The importance for all input/output of welding parameters was selected to be the same (+ + +). Table (6) presents the twelve optimal solutions based on the chosen optimization criteria as determined by Design-Expert software using numerical multiple-response. The ramps view in Fig. (15) exhibits the first optimal solution in Table (11). However, the achieved values for the responses using multiple-response optimization are less than those values obtained by applying the single-response optimization.

Table 11. The twelve optimal solutions using numerical multiple-responses.

No	Current Amp	Speed mm/min	Groove mm	Arc Length (mm)	Microhardness HV	Specific wear rate $mm^3/N.m$	Desirability
1	112.83	100.000	2.500	2.000	1111.789	0.000	0.968 Selected
2	112.99	100.014	2.500	2.000	1108.957	1.899	0.967
3	112.13	100.000	2.463	2.004	1104.021	0.001	0.966
4	112.60	100.006	2.500	2.040	1108.377	0.001	0.963
5	113.17	100.000	2.500	2.020	1102.503	5.103	0.963
6	110.80	100.000	2.386	2.000	1087.438	0.005	0.962
7	110.20	100.000	2.350	2.000	1079.126	0.001	0.960
8	112.22	100.000	2.415	2.000	1078.855	10.737	0.958
9	109.65	100.000	2.319	2.004	1071.097	0.000	0.957
10	109.45	100.000	2.305	2.001	1067.641	0.177	0.956
11	112.54	100.000	2.500	2.115	1095.543	4.306	0.951

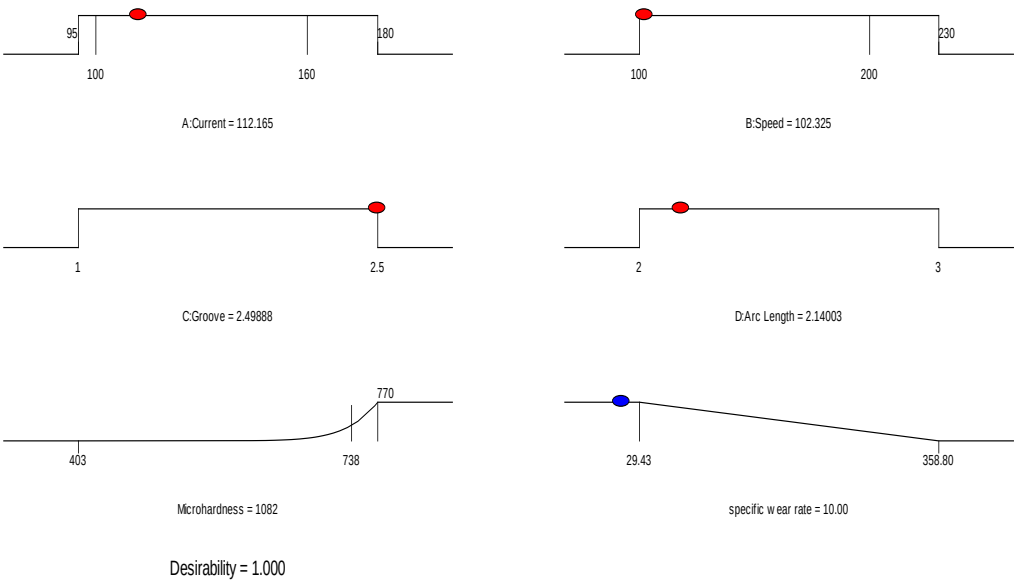

Fig. 15. The desirability for each factor and each response, as well as the combined desirability at the optimal point.

4 Conclusions

Ti / TiC surface coating was produced on CP-Ti using carbon powder filled with different depth and TIG process with different heat input. We obtained high hardness and all specimens are free of cracking.
Surface composite coatings had fairly uniform microstructures through the depth of the coatings and mainly contained primary and dendritic TiC in a martensitic matrix

Increasing heat input, decreased the amount of TiC in the coating which was due to the higher dilution of the process. The selection of lowest current, speed and arc length factors with greater groove depth makes us get the best possible hardness. Where the hardness before the treatment process is measured at 160 HV0.5 . After the treatment process reached 738 HV0.5, which increased by about 4 times (experimentally).

The wear test results showed that the highest hardness specimens containing more TiC When the following factors current = 100 Amperes, speed = 100 mm / min, groove = 2.5 mm and arc length = 2 mm, were the least in terms of loss in the wear test.

The wear resistance of Ti /TiC composite coating was mainly related to its microstructure and primary phase. A ductile matrix, hard TiC particles, homogeneous dispersion of these particles into the matrix and a dense structure with low porosity played dominant roles in the superior wear resistance of the composite coating. The wear resistance improvement was (800%) higher than untreated specimen without any cracking Mathematical models have been developed to connect input parameters with to hardness and wear resistance. 3D dimensional and two-dimensional contour plots were created using computational models developed for hardness and wear resistance. These plots may be useful for predicting responses in any particular combination of any two parameters, while the third and fourth parameters remain constant at one level.

An ANOVA approach was used to determine the levels of importance of input parameters to responses (hardness and wear resistance). Both single-response optimization and multiple-response optimization have been successfully carried out. In single response optimization of Taguchi method using design expert software, the objective is to maximize hardness individually, i.e. separately. The achieved results were based on the different criteria's according to the importance of each parameter (factor) and each response. The predicted hardness was 1460HV0.5 which is about 9 times the untreated value of 160 HV0.5.

In multiple-response optimization of Taguchi method using design expert software, numerical and graphical optimization were used by selecting the desired goals for each parameter (factor) and each response. The numerical multiple-response optimization criterion was to reach, maximize hardness and minimize wear rate. The importance for all inputs/outputs of welding parameters were selected to be the same (+++). The graphical optimization was obtained by the software to define the regions where requirements simultaneously meet the proposed criteria.

Conflict of Interest

This is to certify that all authors have seen and approved the manuscript being submitted and to declare that they have no conflicts of interest..

References

1. ASM handbook, Vol 2-properties and selection: nonferrous alloys and special—purpose materials. ASM International (1990).
2. A. Bloyce, P. Morton, T. Bell, (1994). ASM Handbook, OH, ASM International.
3. H. Huang, K. J. Winchester, A. Suvorova, B. R. Lawn, Y. Liu, X. Z Hu, J. M. Dell, & L. Faraone, (2006). Effect of deposition conditions on mechanical properties of low temperature PECVD silicon nitride films, Materials Science and Engineering: A, vol.435-436, pp.453-459.
4. S. Kumar, T. S. N. Sankara Narayanan, S. Ganesh Sundara Raman, & S. K. Seshadri, (2010), Thermal oxidation of Ti6Al4V alloy: Microstructural and electrochemical characterization, Materials Chemistry and Physics, vol.119, pp.337-346.
5. F.M. Shuaeib, and K.Y. Benyounis, (2016). Advances in Laser Nitriding Methods and Apparatus for Metals and Alloys. In: Saleem Hashmi (editor-in-chief), Reference Module in Materials Science and Materials Engineering. Oxford: Elsevier; 2016. pp. 1-20.

6. F.M. Shuaeib, and K.Y. Benyounis, (2016), An In-depth Investigation of Gas Nitriding of Stainless Steel: New DOE Parametric Studies and Optimization. In: Saleem Hashmi (editor-in-chief), Reference Module in Materials Science and Materials Engineering. Oxford: Elsevier; 2016. pp. 1-12.
7. A. Biswas, & J. Dutta Majumdar, (2009), Surface characterization and mechanical property evaluation of thermally oxidized Ti-6Al-4V. Materials Characterization, vol.60, pp.513-518
8. N. Tsuji, S. Tanaka & T. Takasugi, (2009), Effects of combined plasma-carburizing and shot-peening on fatigue and wear properties of Ti-6Al-4V alloy. Surface and Coatings Technology, vol.203, pp.1400-1405
9. H. Savaloni, K. Khojier & S. Torabi, (2010), Influence of N+ ion implantation on the corrosion and nano-structure of Ti samples. Corrosion Science, vol.52, pp.1263-1267.
10. P. V. Bharathy , D. Chu Nataraj, P. K. Wang, H., Yang, Q. Kiran, M. S. R. N. Silvestre , J. Albero. & D. Mangalaraj, (2010), Effect of titanium incorporation on the structural, mechanical and biocompatible properties of DLC thin films prepared by reactive-biased target ion beam deposition method. Applied Surface Science, vol.257, pp.143-150
11. T.S., Kim, Y.G., Park, & M.Y. Wey, (2003), Characterization of Ti-6Al-4V alloy modified by plasma carburizing process. Materials Science and Engineering A, vol.361, pp.275-280
12. J. H. Lee, N. N. Thadhani, (1997), Reaction synthesis mechanism in dynamically densified Ti+ C powder compacts. Scripta Materialia, vol.37, pp.1979-1985
13. X. Yin, I. Gotman, L. Klinger, & E. Y. Gutmanas, (2005), Formation of titanium carbide on graphite via powder immersion reaction assisted coating. Materials Science and Engineering A, vol.396, pp.107-114.
14. B. Cochepin, V. Gauthier, D. Vrel & S. Dubois, (2007), Crystal growth of TiC grains during SHS reactions. Journal of Crystal Growth, vol.304, pp.481-486.
15. Y. Luo, H. Jiang, G. Cheng & H. Liu, (2011), Effect of carburization on the mechanical properties of biomedical grade titanium alloys. Journal of Bionic Engineering, vol.8,pp.86-89.
16. S. K. Wu, C. Y. Lee & H. C. Lin, (1997), A study of vacuum carburization of an equiatomic TiNi shape memory alloy. Scripta Materialia, vol.37, pp.837-842.
17. A. F. Saleh, J. H. Abboud & K. Y. Benyounis, (2010), Surface carburizing of Ti-6Al-4V alloy by laser melting. Optics and Lasers in Engineering, vol.48, pp.257-267.
18. F. Adib Hajbagheri , S. F. Kashani Bozorg and A. A. Amadeh, Microstructure and wear assessment of TIG surface alloying of CP-titanium with silicon, J Mater Sci (2008) 43:5720–5727, DOI 10.1007/s10853-008-2890-9.
19. A. Monfared, A.H. Kokabi, S. Asgari, (2013), Microstructural studies and wear assessments of Ti/TiC surfacecomposite coatings on commercial pure Ti produced by titanium cored wires and TIG process, Materials Chemistry and Physics, 2013.
20. S. Chatterjee, T.K. Pal, (2003), Wear behaviour of hardfacing deposits on cast iron Wear Volume 255, Issues 16, August–September 2003, Pages 417-425, https://www.sciencedirect.com.
21. C. Fan, M.C. Chen, C.M. Chang, W. Wu, (2006), Microstructure change caused by (Cr, Fe)23C6 carbides in high chromium Fe–Cr–C hardfacing alloys, Surface and Coatings Technology Volume 201, Issues 3–4, 5 October 2006, Pages 908-912, https://www.sciencedirect.com
22. K. H. Zum Gahr, (1998), Wear by hard particles, Tribology International, Volume 31, Issue 10, October 1998, Pages 587-596, https://www.sciencedirect.com.
23. ASTM-G137, Standard Test Method for Ranking Resistance of Plastic Materials to Sliding Wear Using a Block-On-Ring Configuration